Nuclear Engineering and Design 340 (2018) 300–307

Contents lists available at ScienceDirect

Nuclear Engineering and Design

journal homepage: www.elsevier.com/locate/nucengdes

Monte Carlo simulation of PKA distribution along nanowires under ion radiation

Yang Yang[a], Michael P. Short[a], Ju Li[a,b,*]

[a] Department of Nuclear Science and Engineering, Massachusetts Institute of Technology, Cambridge, MA 02139, USA
[b] Department of Materials Science and Engineering, Massachusetts Institute of Technology, Cambridge, MA 02139, USA

ARTICLE INFO

Keywords:
Nanowire
Ion implantation
Irradiation
3D
Monte Carlo simulation
PKA

ABSTRACT

An open-source and full-3D Monte Carlo simulation code, Mat-TRIM, was developed in MATLAB to study the primary knock-on atom (PKA) statistics along nanowires under ion radiation. It is based on TRIM/SRIM's physics; however, compared to TRIM/SRIM, it enables us to properly handle the 3D geometry of a cylindrical nanowire and a planar source of ions. In this paper, we first discuss the mechanism of Mat-TRIM, followed by some validation examples. Then the distributions of ion density, PKA density, PKA total energy, and PKA average energy in nanowires are explored. Significant differences have been found between the slab and the nanowire simulations. The relative error of a 1D slab and the assumption of a point beam source can be more than 1000% when the nanowire is around 20 nm in diameter. In addition, collisions with electrons is demonstrated to be the dominant mechanism of energy loss in narrow nanowires. Our results reveal that full-3D simulations which correctly treat ion leakage at sample boundaries are necessary to properly simulate PKA production in nano-sized targets.

1. Introduction

Recent research has shown some interesting phenomena of the response of nano materials under irradiation. Nanostructured materials, such as carbon-nanotube/metal composites (So et al., 2016), nanoporous materials (Bringa et al., 2012), multilayer nanocomposites (Demkowicz et al., 2008), and oxide dispersion strengthened (ODS) alloys (Sagaradze et al., 2001) have shown superior radiation damage tolerance because of the high volume fractions of robust damage sinks (Azevedo, 2011). Also, in fusion reactors, the helium ion radiation will induce nano-structured fuzz on the surface of the plasma facing materials (PFM), impacting the thermal transport and mechanical performance (Li et al., 2017). In addition, abundant research has been conducted to study the mechanical behavior of nanowires after ion irradiation (Ding et al., 2016; Liontas et al., 2014). Since the volume of a radiation sub-cascade (about 10^3–10^5 nm^3) (Bacon and Diaz de la Rubia, 1994) is close to the diameter of a nanowire, it is interesting to investigate the behavior of nanowires under ion irradiation by computer simulations. However, most rapid and user-friendly computer codes do not by design account for the intricacies of radiation interactions with nanostructures. In this study, we explain and demonstrate a new code to do precisely this.

Molecular dynamics (MD) is widely used to model radiation damage in materials. Traditional MD studies of cascade processes were initiated by giving a selected atom (PKA) a large kinetic energy (Demkowicz et al., 2011). Here, the definition of PKA - Primary Knock-on Atom - is a native atom of the host material that directly collides (generation 1) with the incoming radiation (neutrons in the case of reactors, and accelerated ions in the case of ion accelerators) and gets knocked off its original lattice site, instead of being knocked off by other generation-n ($n \geq 1$) atoms of the host material. PKAs are thus the level-1 nodes of a collision cascade tree, the level-0 root node being that of an external radiation particle. The position/energy distribution of PKAs is often calculated from Monte Carlo simulations, such as TRIM/SRIM (Ziegler et al., 2010). TRIM/SRIM assumes a multilayered structure, with each layer infinitely extending in the x and y directions (see Fig. 1). However, the validity of this assumption is questionable when the characteristic length of the target is comparable to the maximum penetration depth of the ions, which usually ranges from a few nanometers to a few microns. Full-3D simulations become necessary to capture the increasingly large effect of ion leakage out of nanosized features (Yang et al., 2018a). Previously, several Monte Carlo codes have been written to overcome this challenge, such as IM3D (Li et al., 2015), TRI3DYN (Möller, 2014), MyTRIM (Schwen, 2018), Corteo 2D/3D (Schiettekatte and Chicoine, 2016) and iradina (Borschel and Ronning, 2011). Although these codes can handle very complicated structures, their main

* Corresponding author at: Bldg. 24-202, 77 Massachusetts Ave, Cambridge, MA 02139, USA.
E-mail address: liju@mit.edu (J. Li).

https://doi.org/10.1016/j.nucengdes.2018.09.001
Received 1 November 2017; Received in revised form 17 July 2018; Accepted 5 September 2018

Fig. 1. Schematic illustration of TRIM/SRIM's assumptions about beam source and target structure.

focus is on the study of injected/sputtered ions and vacancy distributions, while detailed PKA statistics (for example, PKA energy distributions) are rarely discussed.

Here we develop an open-source and full-3D Monte Carlo code written in MATLAB to study PKA statistics in a target of simple shapes. The code is named Mat-TRIM (Yang et al., 2018b). In the first section of this paper, we introduce how ion-matter interactions are modelled in our code, and present the basic algorithms. The main physics engine is based on Biersack and Haggmark's paper (Biersack and Haggmark, 1980), whose validation examples are also used for Mat-TRIM. In the second section, we will use our model to study PKA statistics along nanowires, assuming a planar ion source entering the material.

2. Methods

Mat-TRIM is based on the binary collision approximation (BCA) model. During the simulation, we model all collision events and movements through the 'life' of each energetic ion. Basically, there are four principal types of charged-particle interactions (Yip, 2014):

(1) Inelastic collisions with atomic electrons
(2) Inelastic collisions with a nucleus
(3) Elastic collisions with a nucleus
(4) Elastic collisions with atomic electrons

(1) is the main process of energy transfer when bremsstrahlung is not significant. (2) is also part of what causes bremsstrahlung, and it only occurs in significant amounts at kinetic energies of at least 10^3 MeV for heavy particles. (3) is known as nuclear stopping, while (4) is only significant for low-energy electrons. In our BCA model, we will only consider (1) and (3), assumed to be independent. We further assume that only (3) will change the direction of incident ions and (1) will only lead to energy loss. Thus, in between two binary nuclear collisions, the ions always move in a straight direction. The total energy loss is therefore a result of both (1) and (3). An ion's history will be terminated when the energy of the ion is sufficiently low such that no more damage or excitation can occur, usually below 5–10 eV. For energy losses by (1) and (3), low, medium, and high energies are treated differently. When the energy is high, an unscreened Coulomb potential properly accounts for (3) and the Bethe-Bloch formula is used for (1) (Eckstein, 1991). However, when the energy is low, (3) becomes more important and the Molière potential is used for (3). What is more, the charged particle is slow enough to capture electrons, and the treatment of Lindhard and Scharff is used. Interpolation by Varelas and Biersack is used in the intermediate energy regime.

We also assume that the target is considered to be amorphous, with atoms uniformly distributed inside the region of study, thus the crystal orientation dependence of the threshold displacement energy is not considered. This neglects any crystallographic effects, such as channeling or focusing. Meanwhile, we assume that all target atoms are stationary. Relativistic effects, important for electron irradiation, are not considered in our model. Furthermore, we ignore all nuclear reactions.

Fig. 2 shows the basic algorithm of Mat-TRIM. The equations used in the simulation and definition of angles are mainly from Biersack and Haggmark's paper (Biersack and Haggmark, 1980). Mat-TRIM is written in MATLAB and it uses the *rand* function to generate uniformly

```
for all particles do
    Initialization of position, direction and energy;
    life←1;
    while life = 1 do
        Calculate reduced energy;
        Calculate stopping;
        Sample the distance travelled between two
        collisions (L) and the impact parameter P;
        Move to new location and save trajectories;
        Calculate electronic energy loss;
        Reduce energy accordingly ;
        if cross boundary then
            move to boundary, change material;
        else if leak then
            life←0;
        else
            /* Collision                    */
            Sample direction;
            Calculate energy loss;
            Reduce energy accordingly ;
            Add tally;
            Kill the particle if E so small;
        end
    end
end
```

Fig. 2. Basic pseudocode algorithm of Mat-TRIM.

distributed random numbers between 0 and 1. The other sampling methods are listed in Biersack and Haggmark's paper (Biersack and Haggmark, 1980). Here we just introduce some details not covered in that paper. The scattering angle θ_L in the laboratory coordinate system is provided by:

$$\mu_L = \begin{cases} \frac{1+(M_2/M_1)\mu_C}{\sqrt{(M_2/M_1)^2+2(M_2/M_1)\mu_C+1}} & \mu_C \neq -1 \\ 0 & \mu_C = -1 \end{cases} \tag{1.1}$$

where:

$$\mu_C = \cos(\theta),\ \mu_L = \cos(\theta_L) \tag{1.2}$$

and the azimuthal scattering angle is sampled by:

$$\phi = 2\pi\xi \tag{1.3}$$

where ξ is a uniformly distributed random number between 0 and 1. We define the directions of the ion before and after scattering as (u, v, w) and (u', v', w'), respectively. They are related by the cosine of the angle between the ion's direction and the x, y, and z axes:

$$u' = \mu u + \frac{\sqrt{1-\mu^2}\,(uw\cos\phi - v\sin\phi)}{\sqrt{1-w^2}} \tag{1.4}$$

$$v' = \mu v + \frac{\sqrt{1-\mu^2}\,(vw\cos\phi + u\sin\phi)}{\sqrt{1-w^2}} \tag{1.5}$$

$$w' = \mu w - \sqrt{1-\mu^2}\,\sqrt{1-w^2}\cos\phi \tag{1.6}$$

Note that when $u = v = 0$, and $w = 1$, the formula above should be:

$$u' = \sqrt{1-\mu^2}\cos\phi \tag{1.7}$$

$$v' = \sqrt{1-\mu^2}\sin\phi \tag{1.8}$$

$$w' = \mu \tag{1.9}$$

For a full-3D simulation, it is significant to compute the distance to the nearest boundary $d_{\min}$. If the sampled distance L is larger than $d_{\min}$, then it is determined that the ion will exit its current material and enter a different one. For the calculation of $d_{\min}$, we use the constructive solid geometry (CSG) method described in the documentation webpage of

OpenMC (MIT, 2011).

We also reused some validation examples of 1D slab and point ion sources (pencil beam) from Biersack and Haggmark's paper. We choose the implantation of B into Si to study the range and ion distribution, due to the plethora of experimental data. Figs. 3 and 4 show that our simulation results match the experimental data from (Hofker et al., 1975) very well. The distribution exhibits the shape of Bragg peak; however, we notice that the peak is left-shifted because our stopping power at low energies is slightly higher than the real value, sharing the same problem as TRIM (Biersack and Haggmark, 1980). Another thing to note is that we ignored the electronic straggling effect in our model, as it contributes little to the ion range.

Visualizing each ion trajectory is important, since together they provide an intuitive understanding of the ion-matter interaction. Thus, we have made videos (See Movies S1 and S2) and figures visualizing the implantation of 100 keV H into C (H → graphite), and implantation of 100 keV H into Au (H → Au) (see Fig. 5).

From these movies and figures we can see not only how each ion moves, but also the mechanisms of stopping at different stages. Some interesting phenomena are noted below:

1. Fig. 5a shows that large angle deflection is a rare event when the ion energy is high, thus the ions travel almost straight at first and gradually change their directions. Most energy loss is attributed to collisions with electrons in the high and intermediate energy regimes. When the energy becomes low enough, nuclear stopping becomes the dominant energy loss mechanism and large angle scattering happens more frequently. This is clearly shown at the tails of the trajectories. All these observations agree well with basic nuclear stopping power theory.
2. Comparing Fig. 5a and b, we see that the range of H in Au is shorter than H in C. This is because the electronic stopping power of H in a higher-Z target is larger. On the other hand, large-angle deflection happens more frequently in Au than C because the mass of Au is much larger than C.

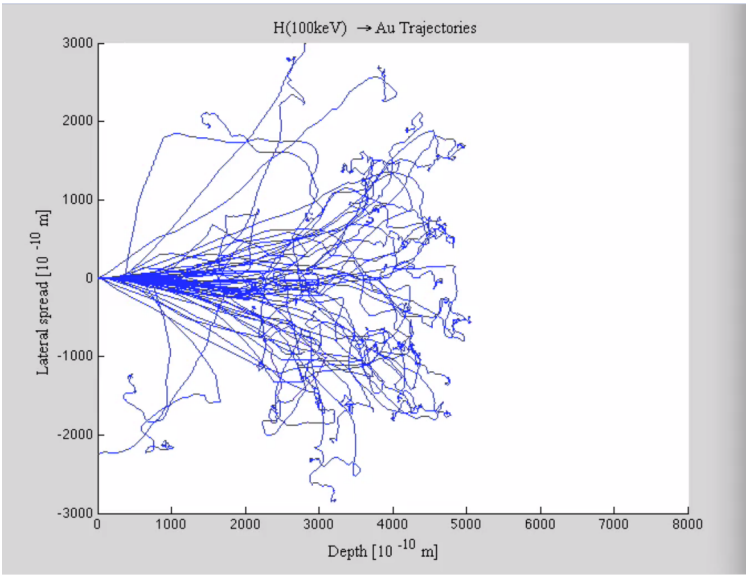

Movie S1.

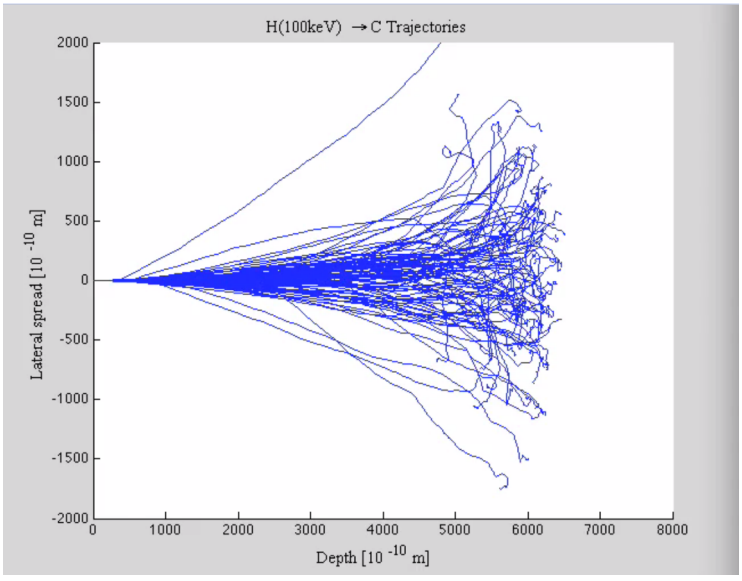

Movie S2.

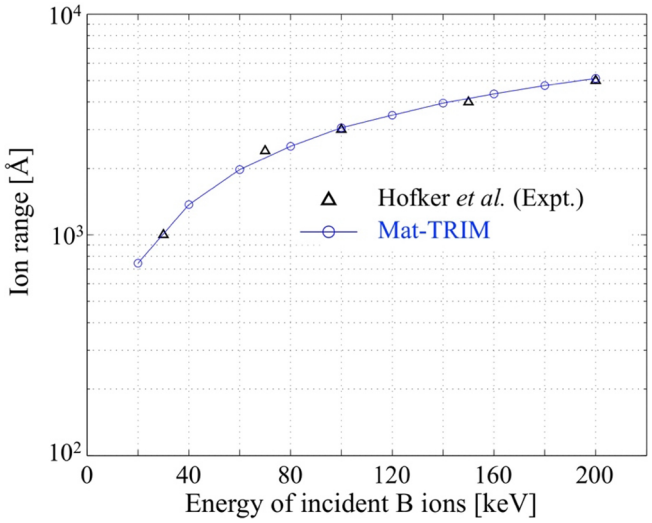

Fig. 3. Ion ranges for implanting B ions of different energies into a Si substrate.

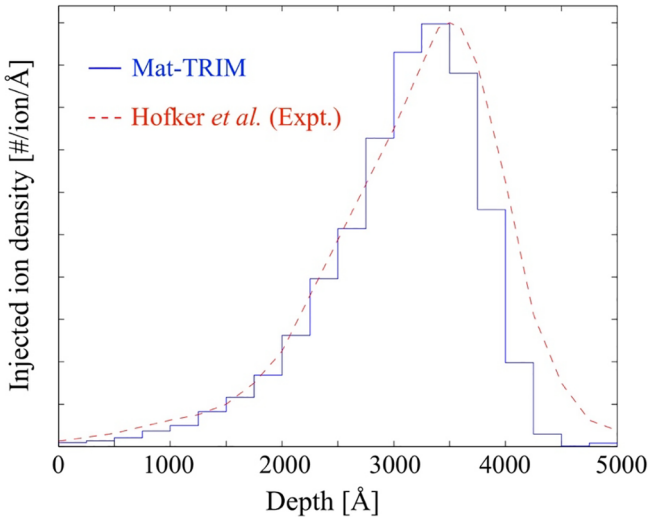

Fig. 4. Distribution of injected B ions in Si, after implantation of B at 100 keV.

3. Results: nanowire study

In this section, we use our model to study PKA trajectories and energy deposition when implanting H into Au nanowires. We are interested in the case where ions bombard the nanowires from the negative-z side, i.e. a plane source in x-y and pointing towards + z. (See Fig. 6).

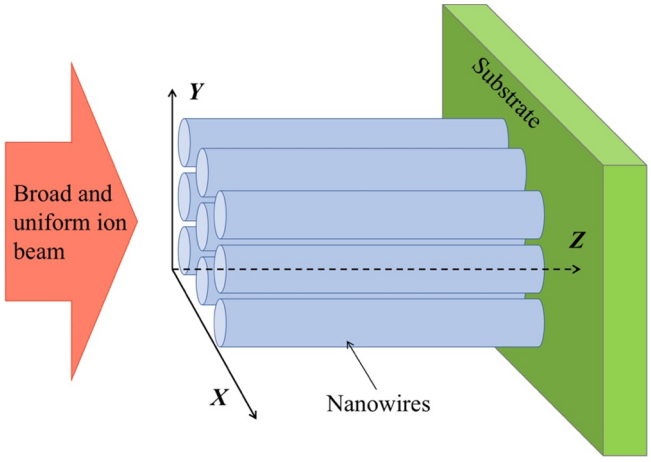

Fig. 6. Schematic illustration of the irradiation and implantation of H ions into Au nanowires.

3.1. PKA density distribution

Before studying H → Au, we first plot the PKA distribution in the 1D semi-infinite slab and point source configurations for 100 keV B → Si in Fig. 7, as a comparison with Fig. 4. The threshold displacement energy for Si is 14 eV (Andersen, 1979). In this paper, if a native atom is hit but does not gain enough energy to be knocked out of lattice, it is not counted as a PKA. The PKA density distribution in 1D slab shows a Bragg peak, which is located slightly shallower than the peak of the injected ion distribution curve. One possible explanation is that when the ion energy loss is lower than the threshold displacement energy, there is no PKA production.

The PKA density distribution along nanowires are studied for 100 keV H → Au for 20 nm and 100 nm diameter (D) nanowires, both using 10^4 ion histories. The times of a single simulation for D = 20 nm and D = 100 nm are 64 s and 157 s, respectively. The threshold displacement energy for Au is 36 eV (Andersen, 1979). When the ion energy is low (in Mat-TRIM, we set the threshold as $E/M_1 < 25$ [keV/amu]), we use Lindard–Scharff formula for the electronic stopping: $S_{\text{electronic}} = c_k k_L E^{1/2}$, where c_k depends on the Z_1 and Z_2. In page 68 of (Eckstein, 1991), Table 5.1, we can find c_k = 1.38 for H into Au. The results are shown in Figs. 8 and 9. Some of the findings are summarized below:

The PKA density distribution along the nanowire is clearly not a simple truncation of that in a 1D slab. The PKA density shows a peak in the entrance and then decreases quickly. The reason may be that we apply vacuum boundary conditions. The ions escape the nanowire

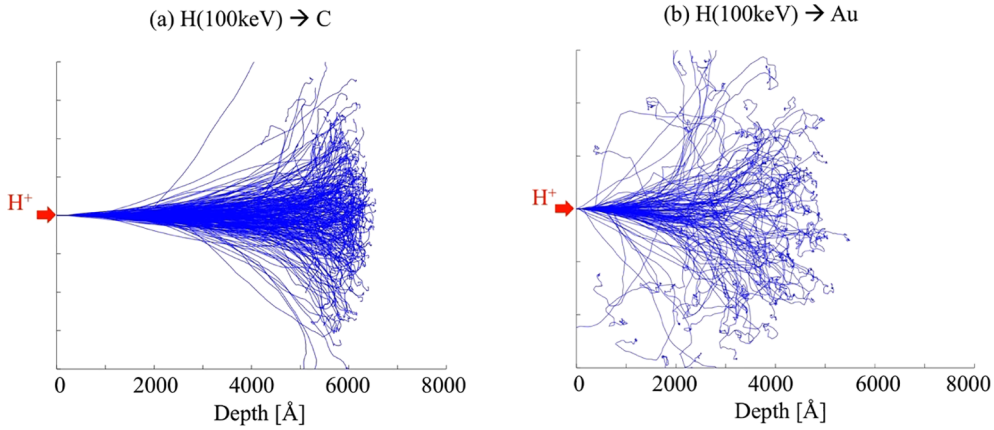

Fig. 5. Ion trajectories for: (a) 100 keV H^+→C; (b) 100 keV H^+→Au. In the same graph, the horizontal axis and vertical axis share the same length scale.

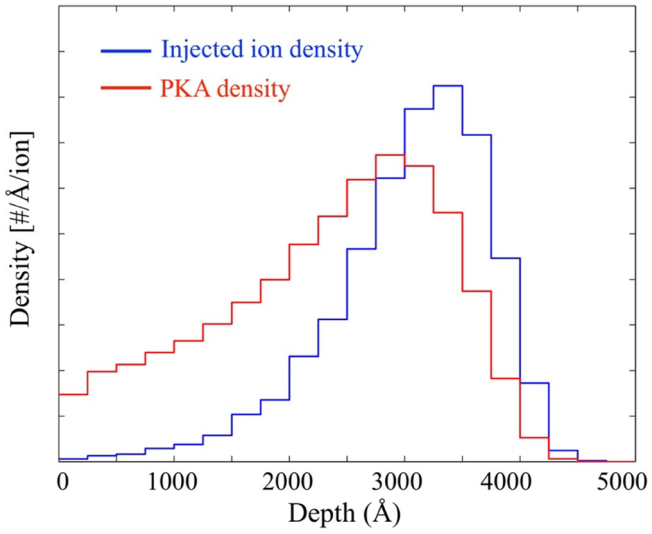

Fig. 7. Injected ion and PKA density distributions for a point beam into a 1D slab for 100 keV B → Si.

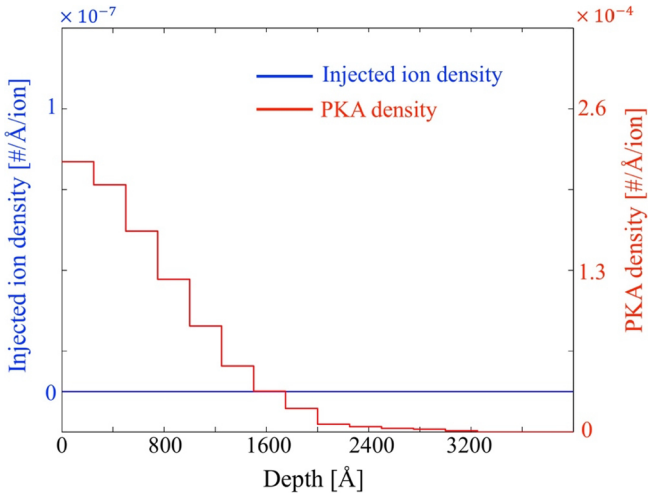

Fig. 8. 100 keV H → Au nanowire (D = 20 nm): PKA density and injected ion distributions along z axis.

quickly within a few scattering events, never to return. This also explains why the PKA density distribution in a nanowire is not a simple truncation of that in a 1D slab, since it does not allow the re-entry of ions after leaking out.

Almost no ions are deposited in the D = 20 nm nanowire. As the nanowire becomes larger in diameter, more and more ions will be stopped inside the nanowire, noting that ions only deposit at deeper positions near the end of their ranges, with greatly varying lateral ranges. The total PKA population in the D = 20 nm nanowire (~3000) is smaller than that in the D = 100 nm nanowire (~8500), out of 10,000 incoming ions. Note that PKA is defined in this paper as those generation-1 atoms that are knocked off their original site, not the ones that are hit but with energy less than the displacement threshold energy. An incoming ion can thus (a) reduce its energy but does not change direction with electronic loss, (b) reduce energy and change direction by sub-displacement threshold collisions that do not create PKA, and (c) reduce energy and change direction by PKA-creating collisions.

3.2. PKA energy distribution

It is also necessary to investigate the average PKA energy (in units of eV) and total energy (average PKA energy × PKA density, in units of

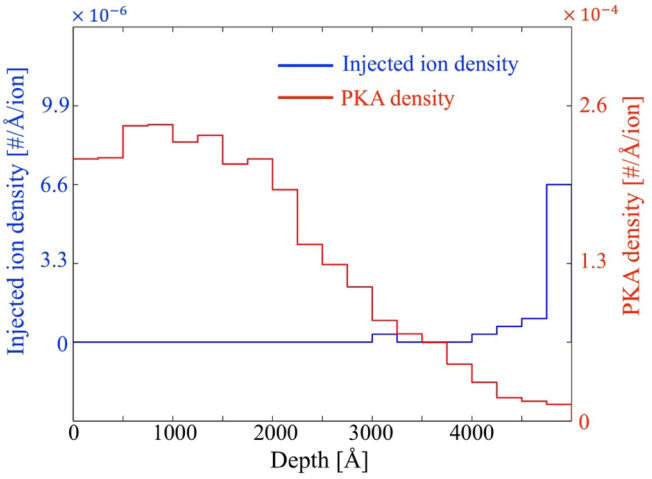

Fig. 9. For 100 keV H → Au nanowire (D = 100 nm): PKA density and injected ion distributions along z axis.

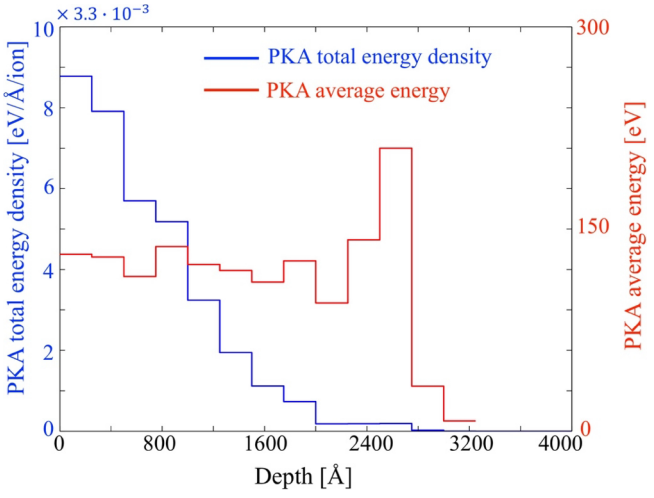

Fig. 10. PKA total energy and PKA average energy distributions along the z-axis (100 keV H → Au, D = 20 nm nanowire).

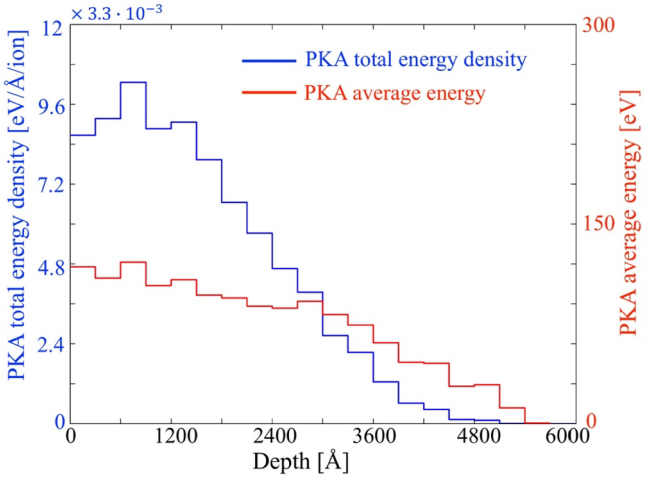

Fig. 11. PKA total energy and PKA average energy distributions along the z-axis (100 keV H → Au, D = 100 nm nanowire).

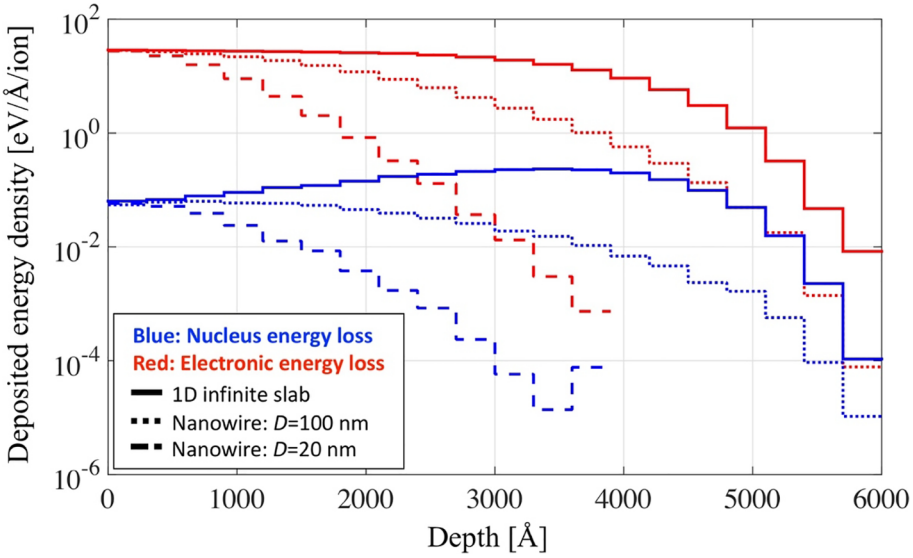

Fig. 12. Electronic/nuclear energy loss comparison for different target geometries for 100 keV H → Au.

eV/length) distributions along nanowires. The results are shown in Figs. 10 and 11, from which we can draw several interesting conclusions:

First, the PKA total energy distribution almost maintains the shape of the PKA density distribution in the $D = 100$ nm nanowire, while that for the $D = 20$ nm nanowire is very different. Second, the PKA average energy distribution is nearly constant in 20 nm diameter nanowires, except for the deepest region where there is significant statistical noise. However, in the $D = 100$ nm nanowire, the PKA average energy decreases gradually. It is reasonable since the ions travel deeper in the $D = 100$ nm nanowire, and suffer more collisions and energy losses due to a lower probability of leaving the free surface as a function of depth.

3.3. Energy loss comparison

Here we compare energy losses due to collisions with electrons and nuclei in Fig. 12. Interestingly, the phenomena at different scales are quite different:

For 1D slab (bulk case): when the incoming ion energy is high (i.e., near the entrance), electronic energy loss is about three orders of magnitude higher than the nuclear energy loss; when the ion energy is low enough (i.e., near the end of its range), there is a larger drop in electronic energy loss and thus the difference between nuclear energy loss and electronic energy loss is smaller. The energy loss due to elastic scattering first increases, and then decreases as the ions travel deeper. However, for a nanowire, it is striking that electronic energy loss is always about three orders of magnitude larger than nuclear energy loss, and both of them decrease as the ion depth increases. The reason for the relatively stable electronic loss / nuclear loss ratio is that the kinetic energy of ions stays high in the nanowire. For the $D = 100$ nm nanowire, 99.77% ions leak with an average energy of 47.8 keV; while for the $D = 20$ nm nanowire, nearly 100% ions leak with an average energy of 75.0 keV. Larger deflection means larger elastic energy loss, and those ions undergoing larger deflection have a higher chance of leakage. Thus, the conditional probability is such that the ions which have stayed inside a narrow nanowire tend to have higher energy (and fewer prior collisions), causing the electronic loss to maintain its dominance until the end of the ion's range. This might have implications if one uses nanowires in spatially resolved radiation detectors. Also, it suggests that electronic energy loss is significant in

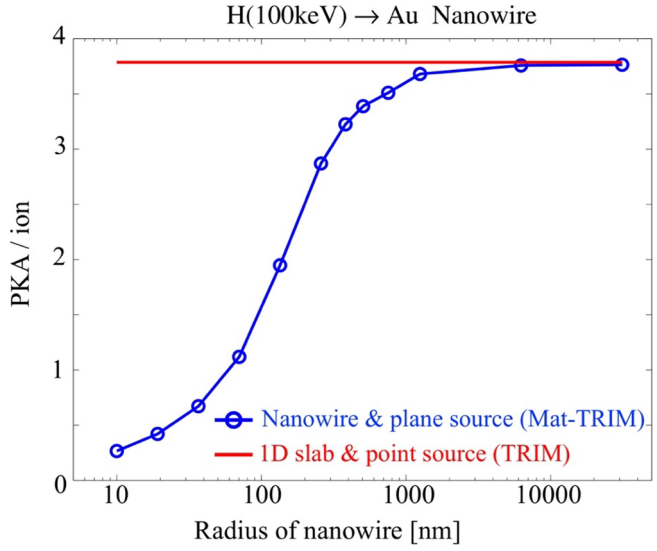

Fig. 13. Comparison between Mat-TRIM and the 1D slab and point source approximation with TRIM/SRIM.

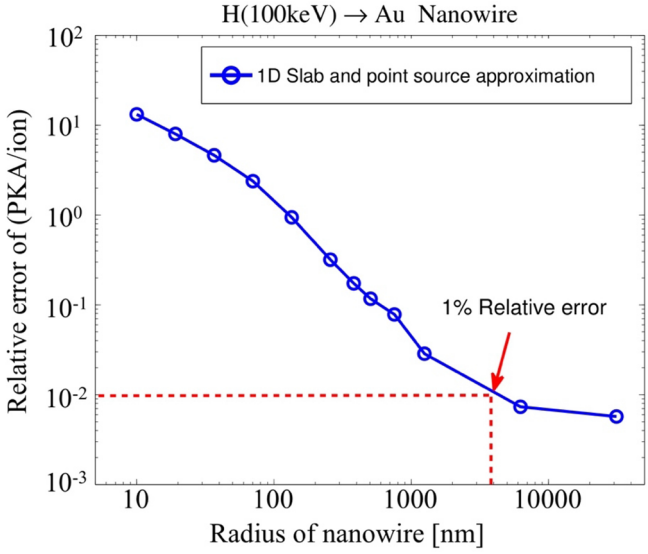

Fig. 14. Relative error of 1D slab and point source approximation for calculation of total PKA in a cylinder.

nanostructured systems. The effect of electrons is usually neglected in MD simulations of radiation damage cascades if the PKA energy is low (Rutherford and Duffy, 2007). However, from our results in Figs. 10–12, it has been shown that the PKA energy is kept high in the nanowires, and electronic energy loss is always dominant. Therefore, one should consider the electronic energy loss term in the MD simulation of radiation damage in nanowires.

3.4. 1D slab and point source approximation

Finally, we consider when we could safely use the 1D slab and point source approximation (TRIM) without the above effects altering the result. Fig. 13 shows that as the radius of the cylinder increases, the total PKA population approaches the result of the 1D slab and point source scenario, which could be solved by TRIM. The relative error between the two cases is shown in Fig. 14. We can see that when the radius of cylinder is larger than 3.5 μm, the relative error is below 1%, and the 1D slab and point source could be a good approximation. When the radius is below 3.5 μm, the relative error will increase dramatically as the nanowire radius decreases. In this case, one cannot trust the 1D slab and point-source approximation anymore, and a more accurate 3D model (for example, Mat-TRIM) should be used instead. Note that the criteria of using full-3D simulations relies on the ion energy, ion type and the target properties. Also, when the target is too small (usually below 20 nm), another effect named “nano-energetic effect” (Li et al., 2015) emerges as the stopping power and the displacement threshold energy for bulk materials may lose their validity.

4. Discussion and conclusion

In this report, we have presented a Monte Carlo simulation algorithm with our BCA model, focusing on the illustration of nanoscale effects and highlighting differences between nanowire and bulk irradiations. Unlike some existing BCA codes which can only solve 1D slab and point source problems, our code Mat-TRIM enables the simulation of cylindrical geometries on the nanoscale with a more experimentally-representative planar ion source. Using Mat-TRIM, we study PKA statistics along differently sized nanowires under ion irradiation. Interesting phenomena concerning the irradiation of nanowires are discovered through our simulations, which differ from the macroscale case (1D slab) in the following ways:

1. The PKA density decreases from the entrance in a narrow nanowire, while the PKA distribution in the 1D infinite slab first increases, then decreases.
2. Ion injection decreases drastically for a smaller nanowire, due to scattered ions leaving free surfaces and not returning.
3. In small nanowires ($D = 20$ nm), the PKA average energy distribution is very uniform.
4. In a 1D slab, the energy loss due to elastic scattering will first increase, and then decrease as the depth increases; while in nanowires, it always decreases. Therefore, in small nanowires, the electronic energy loss is always dominant, indicating that MD simulations of cascade in small-scale systems should account for the electronic energy loss term.

We have shown that the 1D slab and point source approximation using TRIM loses its validity when the radius of the object being irradiated is below a certain value (3.5 μm for 100 keV H^+ implantation in Au). It reveals the non-negligible target size effects of ion implantation. Therefore, full-3D Monte Carlo simulations are necessary for accurate PKA calculations in nanostructured materials.

5. Notes

The authors declare no competing financial interests.

6. Author contributions

Y.Y. and J.L. conceived of the project. Y.Y. wrote the code and performed the simulations. M.P.S. and Y.Y. conceived of the relative error analysis method. All authors analyzed the data, contributed to the discussion, and wrote the manuscript.

7. Data availability

The data that support the findings of this study are available from the corresponding authors on request. For ease of validation, the MATLAB source code (Mat-TRIM) is permanently hosted at GitHub (https://github.com/skfreedom/MATLAB-TRIM-3D).

Acknowledgment

The authors thank Prof. Jeremy Roberts from Kansas State University, Dr. Yonggang Li from the Institute of Solid State Physics of the Chinese Academy of Sciences, and Mr. Feng Zhou from McMaster University for helpful discussions.

References

Andersen, H.H., 1979. The depth resolution of sputter profiling. Appl. Phys. 18, 131–140. https://doi.org/10.1007/BF00934407.
Azevedo, C.R.F., 2011. Selection of fuel cladding material for nuclear fission reactors. Eng. Fail. Anal. 18, 1943–1962. https://doi.org/10.1016/j.engfailanal.2011.06.010.
Bacon, D.J., Diaz de la Rubia, T., 1994. Molecular dynamics computer simulations of displacement cascades in metals. J. Nucl. Mater. 216, 275–290. https://doi.org/10.1016/0022-3115(94)90016-7.
Biersack, J.P., Haggmark, L.G., 1980. A Monte Carlo computer program for the transport of energetic ions in amorphous targets. Nucl. Instrum. Meth. 174, 257–269. https://doi.org/10.1016/0029-554X(80)90440-1.
Borschel, C., Ronning, C., 2011. Ion beam irradiation of nanostructures - A 3D Monte Carlo simulation code. Nucl. Instrum. Meth. Phys. Res. Sect. B Beam Interact. Mater. At. 269, 2133–2138. https://doi.org/10.1016/j.nimb.2011.07.004.
Bringa, E.M., Monk, J.D., Caro, A., Misra, A., Zepeda-Ruiz, L., Duchaineau, M., Abraham, F., Nastasi, M., Picraux, S.T., Wang, Y.Q., Farkas, D., 2012. Are nanoporous materials radiation resistant? Nano Lett. 12, 3351–3355. https://doi.org/10.1021/nl201383u.
Demkowicz, M.J., Hoagland, R.G., Hirth, J.P., 2008. Interface structure and radiation damage resistance in Cu-Nb multilayer nanocomposites. Phys. Rev. Lett. 100, 2–5. https://doi.org/10.1103/PhysRevLett. 100.136102.
Demkowicz, M.J., Anderoglu, O., Zhang, X., Misra, A., 2011. The influence of Σ3 twin boundaries on the formation of radiation-induced defect clusters in nanotwinned Cu. J. Mater. Res. 26, 1666–1675. https://doi.org/10.1557/jmr.2011.56.
Ding, M.S., Du, J.P., Wan, L., Ogata, S., Tian, L., Ma, E., Han, W.Z., Li, J., Shan, Z.W., 2016. Radiation-induced helium nanobubbles enhance ductility in submicron-sized single-crystalline copper. Nano Lett. 16, 4118–4124. https://doi.org/10.1021/acs.nanolett.6b00864.
Eckstein, W., 1991. Computer simulation of ion-solid interactions. Springer Series in Materials Science. Springer Berlin Heidelberg, Berlin, Heidelberg 10.1007/978-3-642-73513-4.
Hofker, W.K., Oosthoek, D.P., Koeman, N.J., de grefte, H.A.M., 1975. Concentration profiles of boron implantations in amorphous and polycrystalline silicon. Radiat. Eff. 24, 223–231. https://doi.org/10.1080/00337577508240811.
Li, Y.G., Yang, Y., Short, M.P., Ding, Z.J., Zeng, Z., Li, J., 2015. IM3D: a parallel monte carlo code for efficient simulations of primary radiation displacements and damage in 3D geometry. Sci. Rep. 5, 18130. https://doi.org/10.1038/srep18130.
Li, Y., Yang, Y., Short, M.P., et al., 2017. Ion radiation albedo effect: Influence of surface roughness on ion implantation and sputtering of materials. Nucl. Fusion 57, 16038. https://doi.org/10.1088/1741-4326/57/1/016038.
Liontas, R., Gu, X.W., Fu, E., Wang, Y., Li, N., Mara, N., Greer, J.R., 2014. Effects of helium implantation on the tensile properties and microstructure of Ni73P27 metallic glass nanostructures. Nano Lett. 14, 5176–5183. https://doi.org/10.1021/nl502074d.
MIT, 2011. OpenMC: Theory and Methodology [WWW Document]. URL https://openmc.readthedocs.io/en/stable/methods/index.html.
Möller, W., 2014. TRI3DYN–Collisional computer simulation of the dynamic evolution of 3-dimensional nanostructures under ion irradiation. Nucl. Instrum. Methods Phys. Res. B: Beam Interact. Mater. Atoms 322, 23–33.
Rutherford, A.M., Duffy, D.M., 2007. The effect of electron-ion interactions on radiation damage simulations. J. Phys.: Condens. Matter 19. https://doi.org/10.1088/0953-8984/19/49/496201.
Sagaradze, V.V., Shalaev, V.I., Arbuzov, V.L., Goshchitskii, B.N., Tian, Y., Qun, W., Jiguang, S., 2001. Radiation resistance and thermal creep of ODS ferritic steels. J. Nucl. Mater. 295, 265–272.
Schiettekatte, F., Martin, C., 2016. Spectrum simulation of rough and nanostructured targets from their 2D and 3D image by Monte Carlo methods. Nucl. Instrum. Methods Phys. Res. B: Beam Interact. Mater. Atoms 371, 106–110.

Schwen, D., 2018. MyTRIM [WWW Document]. https://github.com/idaholab/mytrim.
So, K.P., Chen, D., Kushima, A., Li, M., Kim, S., Yang, Y., Wang, Z., Park, J.G., Lee, Y.H., González, R.I., 2016. Dispersion of carbon nanotubes in aluminum improves radiation resistance. Nano Energy 22, 319–327.
Yang, Y., Li, Y.G., Short, M.P., et al., 2018a. Nano-beam and nano-target effects in ion radiation. Nanoscale 1598–1606.
Yang, Y., Short, M., Li, J., 2018. Mat-TRIM [WWW Document]. https://github.com/skfreedom/MATLAB-TRIM-3D.
Yip, S., 2014. Nuclear Radiation Interactions. World Scientific Publishing Co Inc.
Ziegler, J.F., Ziegler, M.D., Biersack, J.P., 2010. SRIM - The stopping and range of ions in matter. Nucl. Instrum. Meth. Phys. Res. Sect. B Beam Interact. Mater. At. 268, 1818–1823. https://doi.org/10.1016/j.nimb.2010.02.091.